Nascent β Structure in the Elongated Hydrophobic Region of a Gerstmann–Sträussler–Scheinker PrP Allele

Ze-Lin Fu[1,2], Peter C. Holmes[2], David Westaway[1,2] and Brian D. Sykes[2]

*1 - **Centre for Prions and Protein Folding Diseases,** University of Alberta, Edmonton, Alberta, Canada T6G 2M8*
*2 - **Department of Biochemistry,** University of Alberta, Edmonton, Alberta, Canada T6G 2H7*

***Correspondence to Brian D. Sykes:** brian.sykes@ualberta.ca.*
https://doi.org/10.1016/j.jmb.2019.04.027
Edited by C. Kalodimos

Abstract

Prion diseases are neurodegenerative disorders caused by the misfolding of the cellular prion protein (PrP^C). Gerstmann–Sträussler–Scheinker syndrome is an inherited prion disease with one early-onset allele (HRdup) containing an eight-amino-acid insertion; this LGGLGGYV insert is positioned after valine 129 (human PrP^C sequence) in a hydrophobic tract in the natively disordered region. Here we have characterized the structure and explored the molecular motions and dynamics of HRdup PrP and a control allele. High-resolution NMR data suggest that the core of HRdup has a canonical PrP^C structure, yet a nascent β-structure is observed in the flexible elongated hydrophobic region of HRdup. In addition, using mouse PrP^C sequence, we observed that a methionine/valine polymorphism at codon 128 (equivalent of methionine/valine 129 in human sequence) and oligomerization caused by high protein concentration affects conformational exchange dynamics at residue G130. We hypothesize that with the β-structure at the N-terminus, the hydrophobic region of HRdup can adopt a fully extended configuration and fold back to form an extended β-sheet with the existing β-sheet. We propose that these structures are early chemical events in disease pathogenesis.

Introduction

Prion infections are caused by the misfolding of cellular form of the prion protein, PrP^C into an aggregation-prone pathogenic form commonly referred to as PrP^{Sc} [1]. Encoded by the *PRNP* on chromosome 20 in humans [2], PrP^C is a glycosyl-phosphatidylinositol-anchored protein highly expressed in neurons. It consists of a structured, C-globular domain (residues 127–231, mouse numbering) and a flexible, unstructured N-terminus (residues 23–126). The structured C-terminus contains three α-helices and an antiparallel β-sheet [3], while the intrinsically disordered N-terminus features an octarepeat region, which is associated with metal ion binding [4] and also a conserved hydrophobic region (HR). While there have been speculations on the functions of PrP^C that include associations with copper homeostasis, given its ability to coordinate copper ions [5], this remains an active area of research.

Production of misfolded PrP may be initiated under a number of conditions, these including the inheritance of germline mutations. Thus, Gerstmann–Sträussler–Scheinker (GSS) disease is the prototype form of genetic prion disease; it is an autosomal dominant multi-systemic neurological syndrome that can develop into frank dementia and with the patients commonly displaying a protracted clinical course [6]. GSS can arise from a range of mutations within the open reading frame of *PRNP* gene. These mutations are associated with different clinical presentation, yet the most common clinical phenotypes include cerebellar ataxia and pyramidal signs admixed with cognitive decline [7].

One notable *PRNP* mutation discovered recently contains a 24-nucleotide insertion, which encodes an 8-amino-acid internal duplication of the residues LGGLGGYV in the PrP HR (residue 110–130). This mutant allele is referred to as HRdup [8] and occurs in *cis* to valine at codon 129 in *PRNP*, with a common M129 V polymorphism being present in

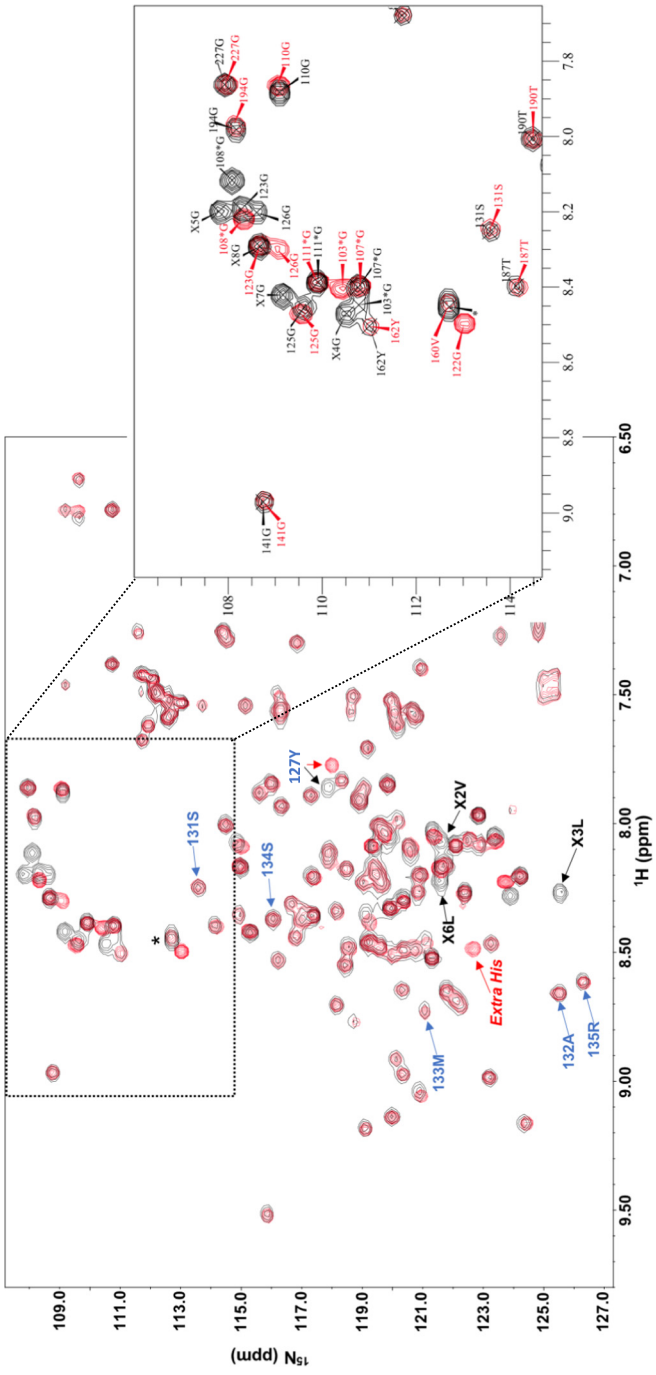

Fig. 1. Superimposition of ^{1}H–^{15}N 2D HSQC NMR spectra of V128 (red) and HRdup (black). The asterisk symbol indicates an overlap of two resonances in the ^{1}H–^{15}N 2D HSQC NMR spectrum of HRdup; the blue arrows show resonances that exist on both spectra, while the red and black arrows indicate resonances that are unique on the spectrum of V128 and HRdup, respectively. The residues with asterisk in the numbering are from the residues artificially added in between the N-terminal His-tag and TEV cleavage site (discussed in Materials and Methods section).

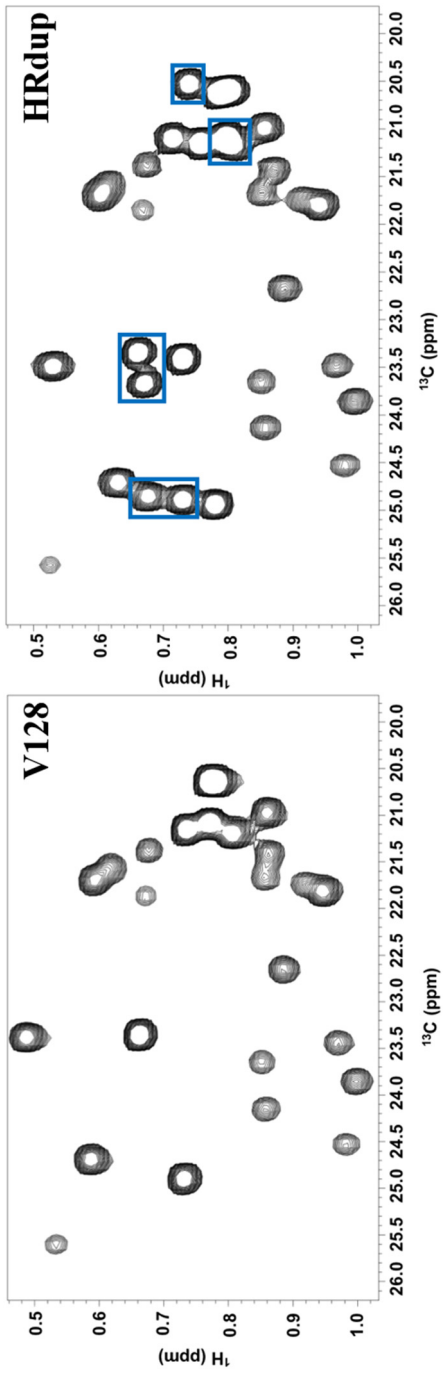

Fig. 2. Expanded methyl region of 2D ^{1}H, ^{13}C-HSQC NMR spectra of V128 (left) and HRdup (right); the extra resonances on the HRdup spectrum (indicated by blue square boxes) correspond to the methyl groups from the extra two leucine and one valine residues from the insert of HRdup.

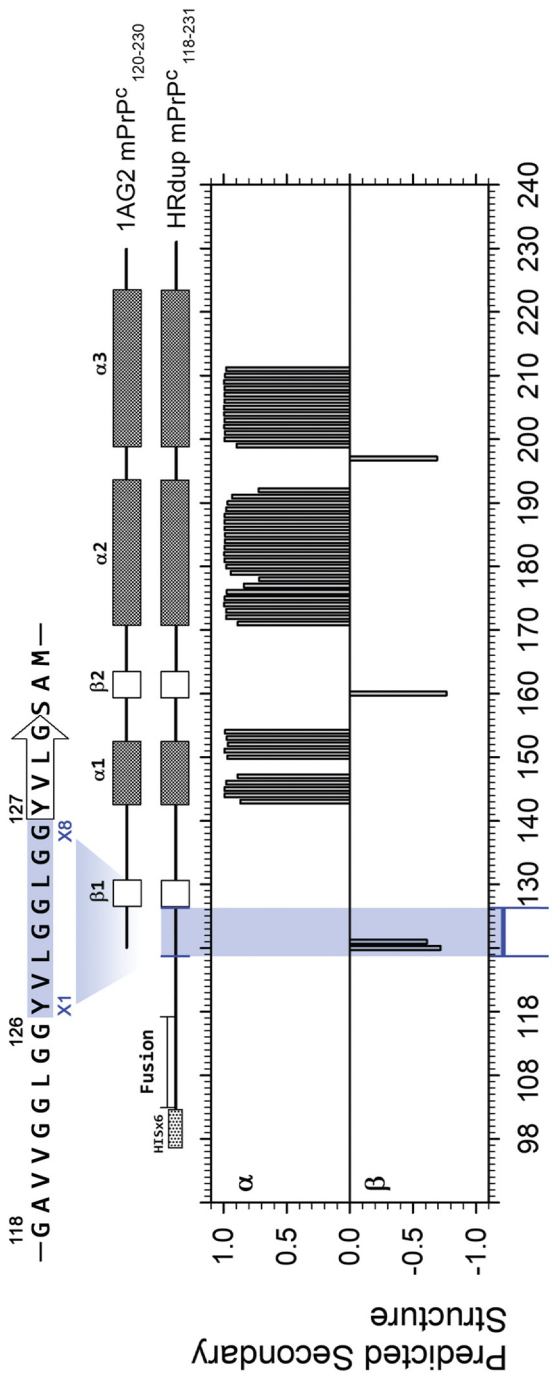

Fig. 3. Top panel shows the sequence numbering of the HR of HRdup; the residues corresponding to the extra resonances on the NMR spectra due to the insertion are numbered X1 to X8. Lower panel shows the secondary structure prediction of HRdup from TALOS+. The canonical secondary structure is shown at the top of the plot (BMRB ID: 1AG2) [13]. All the sequences are aligned by the C-terminus. The residues with high propensity to be α-helices are indicated with positive values, while the residues with high propensity to be β-structures are indicated with negative values.

many human populations [9]. Previous studies have revealed that thermolysin digestion of brain homogenates transgenic (Tg) mice expressing the HRdup allele yields a 16-kDa thermolysin-resistant signature fragment. This fragment derives from the N-terminal and central HR of the HRdup form of PrP [10] and in turn comprises a potential precursor to the observed 8-kDa PK-resistant fragment that is a common feature of most types of GSS disease [11].

Prior analyses have demonstrated that the insertion in HRdup does not disrupt the canonical antiparallel β-sheet present in wild-type (WT) PrP or affect the structural stability of the globular domain of HRdup [10], leaving the structural perturbations that can lead to the spontaneous misfolding and assembling of HRdup unidentified. In this study, we have used high-resolution multinuclear NMR spectroscopy to compare the structures and explore the molecular motions and dynamics of WT mouse PrP^C (118–231, M128; that is, methionine at residue 128 equivalent to human residue M129), mouse PrP^C (118–231) V128, and mouse PrP^C (118–231) V128 HRdup (henceforward referred to as WT, V128, and HRdup, respectively). Our data suggest that while the core of HRdup has a canonical PrP^C structure, a nascent β-structure was observed in the elongated HR of HRdup, a region that is natively unstructured in the M128 and V128 forms of mouse PrP. We also observed that the exchange dynamics of glycine 130 are correlated with methionine/valine polymorphisms at codon 128 and the propensity to form PrP oligomers by high protein concentration. We hypothesize that the newly discovered, nascent β-structure initiates long-range alterations that convert PrP's N-terminal unstructured region into β-enriched forms that resist digestion by thermolysin and proteinase K.

Results

NMR spectra of V128 and HRdup versions of mouse PrP

In general, the 2D $^1H,^{15}N$-HSQC NMR spectrum of a protein is one of the most sensitive indicators of the structure and dynamics of the protein. The 2D $^1H,^{15}N$-HSQC NMR spectra of WT, V128, and HRdup under these same experimental conditions are presented in Supplementary Figs. S1–3. The M128 (WT) and V128 proteins have very similar 2D $^1H,^{15}N$-HSQC NMR spectra, and the spectrum of WT mouse PrP was comparable to previous studies [12].

The solubility of HRdup PrP was found to be highly sensitive to pH and to reach high enough concentration (~0.1 mM) for NMR analysis, pH 4.0~5.0 was used for all the following studies. Despite of the high environmental sensitivity of the amide NH resonances, where even minor differences in sample condition can cause obvious chemical shift changes on spectra, only a few resonances from V128 were shifted *versus* the 2D $^1H,^{15}N$-HSQC NMR spectrum of HRdup (Fig. 1); these were mainly attributed to glycines in the flexible HR that includes the LGGLGGYV insert. These glycines (including the extra 4 glycine resonances due to the insert in HRdup) are shown in detail in Fig. 1. In the 2D $^1H,^{13}C$-HSQC NMR spectra of HRdup, a total of six extra methyl groups were observed *versus* V128 as expected from the methyl groups of two leucines and one valine present in the insert (Fig. 2).

In summary, we observe that the resonances on the spectra of V128 remain at very similar, if not identical chemical shifts to HRdup, while the additional resonances of HRdup appear as "extra" peaks on the spectra. This suggests that even with an insert in its sequence, the core of the HRdup protein adopts the canonical PrP globular domain fold, as does V128 mPrP (118–231).

Chemical shift assignment and novel β-structure detected in HRdup (118–231)

NMR resonances corresponding to amino acids in the N-terminal region of the HRdup construct proved challenging to assign because of the highly repetitive sequence of the HR of HRdup (mPrP 121–128 plus the insert) and its intrinsically disordered nature. The backbone chemical shift assignments (HN, N, C_α and C_β nuclei) were completed to 80% with 3D CACBCONNH and NHCACB NMR spectra. The assignment for HRdup from V124 through the sixth resonance of the insert is shown in Supplementary Fig. S4. For clarity when dealing with duplicated sequences, for the following text, we used a nomenclature scheme (Fig. 3a) where the amino acids attributed to the additional resonances (i.e., those absent from analyses of the control V128 allele) are denoted as "X." ("X" stands for "extra"). Note that this scheme is different from the assignment of extra amino codons as assigned from inspection of the nucleotide sequence of the HRdup *PRNP* allele [8].

Chemical shifts of NH, N, C_α, and C_β nuclei were loaded into TALOS+ program to calculate the secondary structure propensity of HRdup [14] (Fig. 3), with only the assigned residues with a high propensity (>0.5) presented. Residues with high α-helix propensity make up three α-helices, consistent with the helices in WT mPrP. Due to broadening of the resonances from residues in the anti-parallel β-sheet (HRdup 127–130) caused by chemical exchange (see below), the canonical β structure of PrP cannot be completely characterized in this analysis. It has been previously reported that the

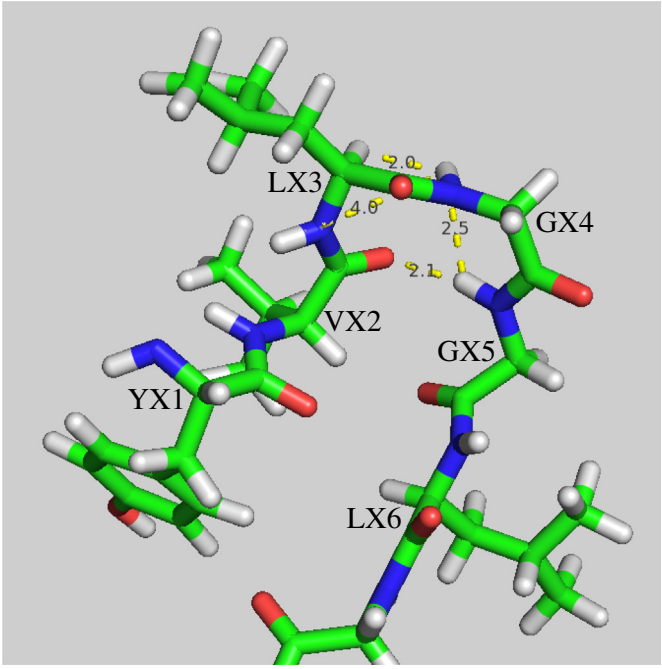

Fig. 4. Snapshot of MD simulation trajectory shows the novel β-structure that is consistent with NMR data and the proposed type 2 β-turn structure. This structure was taken from state No. 728 (out of 5001 states) in the 50-ns trajectory 3 of HRdup [10].

chemical shifts of the residues forming the first β-strand do not possess strong β character [15], but the presence of this canonical β-sheet in HRdup was already demonstrated strongly by $d_{\alpha\alpha}$(L129, Y161) and $d_{\alpha\alpha}$(Y127, R163) nOe's observed in our previously published data [10].

Using the SEQSEE program [16], the residues VX2, LX3, GX4, and GX5 are predicted to have high β-propensity, while the proceeding and following sequences are predicted to be random coil (data not shown). The data set of BetaTPred 3.0 consists of 20,142 protein chains (BT20142); the sequence VLGG is present in total of 220 counts, and in 71 out of 220 counts, a β-turn is formed by VLGG [17]. Consistent with these β-propensity prediction approaches, the most interesting feature of the TALOS+ analysis is a novel high β-propensity structure at valine X2 (VX2) and leucine X3 (LX3) (Fig. 3), indicating that a nascent β-structure is at the highly flexible N-terminus (see following section) of HRdup.

We did not observe the nOes between the residues with high β-propensity making contacts with the existing β-sheet. Rather, we propose that this high β-propensity structure is a nascent β-turn formed by valine at X2 (VX2), leucine at X3 (LX3), and glycine at X4 (GX4). In the 3D NHSQC-NOESY spectrum, we observe the $d_{NN}(i, i+1)$ nOes that are consistent with a type 2 β-turn, where the NH of GX4 points at the carbonyl group of GX5 [18] (Supplementary Fig. S5).

In our previous molecular dynamics (MD) simulation analysis using HRdup fragment from residue 118 to 231 [10], this nascent β-turn existed in all three trajectories of HRdup and the structure(s) observed is consistent with the proposed type 2 β-turn. The MD simulation also shows the flexible and dynamic feature of this novel β-structure. Figure 4 presents a snapshot of VX2, LX3, GX4 and GX5 forming a type 2 β-turn at 7.28 ns in trajectory 3 of HRdup (50 ns in total).

N-terminus ^{15}N relaxation measurements

The ^{15}N transverse (R_2) relaxation rates were measured to gain insight into the backbone motions of the WT, V128 and HRdup alleles. Given that the dynamics of the N-terminus is of the most interest, R_2 values of the residues 118 to 155 of the three alleles are presented (Fig. 5).

The region from residue 119 to 125 is flexible in all three alleles, as indicated by R_2 values $<10\ s^{-1}$. These values are typical for intrinsically disordered parts of proteins [8]. The extra residues of HRdup at the N-terminus are also flexible given their small R_2 values; the aforementioned nascent β-structure in this region does not appear to hinder the flexibility of the backbone in this region. Starting from residue 127 the three alleles become structured, supported by the increased R_2 values resulting from the slow rotational tumbling of the structured core of the protein. The typical value of R_2 for the structured

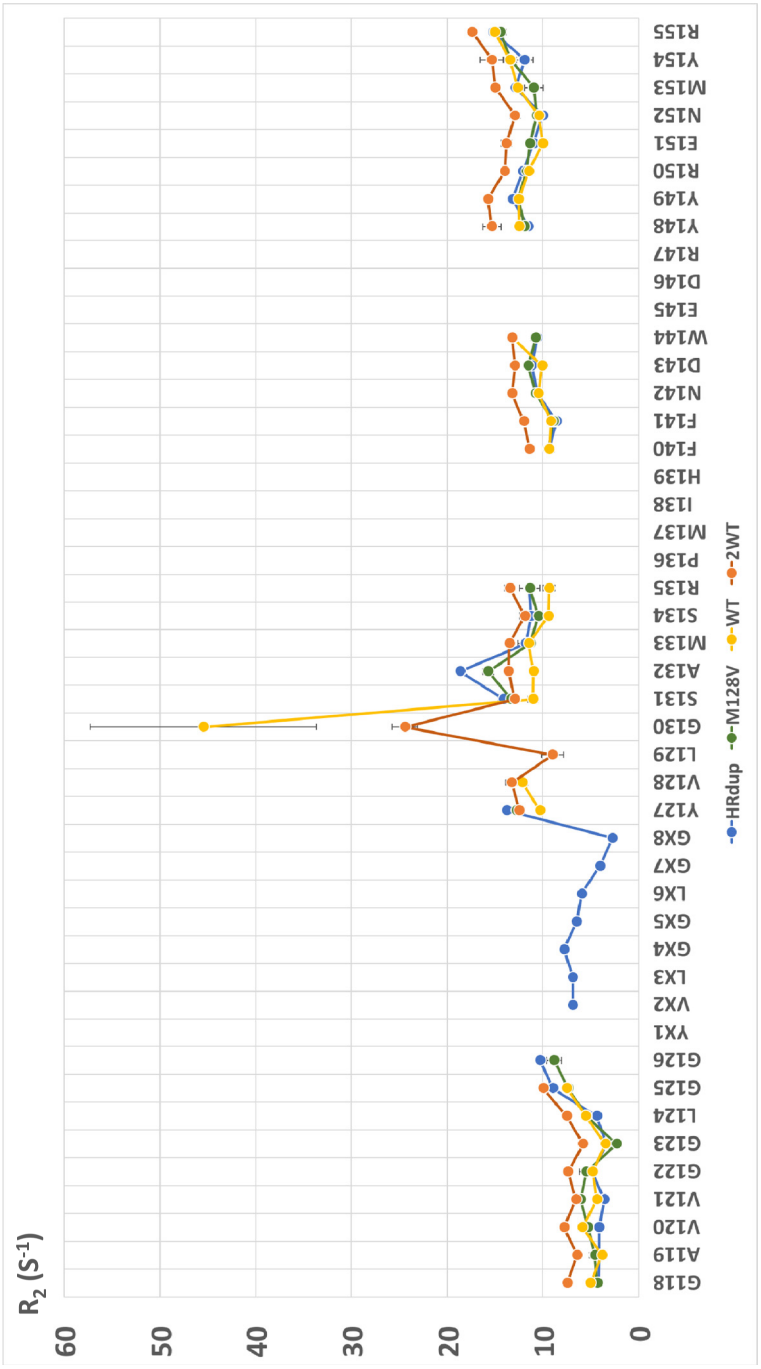

Fig. 5. ^{15}N R_2 relaxation data for 0.1 mM HRdup (blue), 0.1 mM V128 (green), 0.1 mM WT (yellow), and 0.2 mM WT (orange). The gaps are due to overlapping of resonances or missing resonances due to chemical exchange broadening.

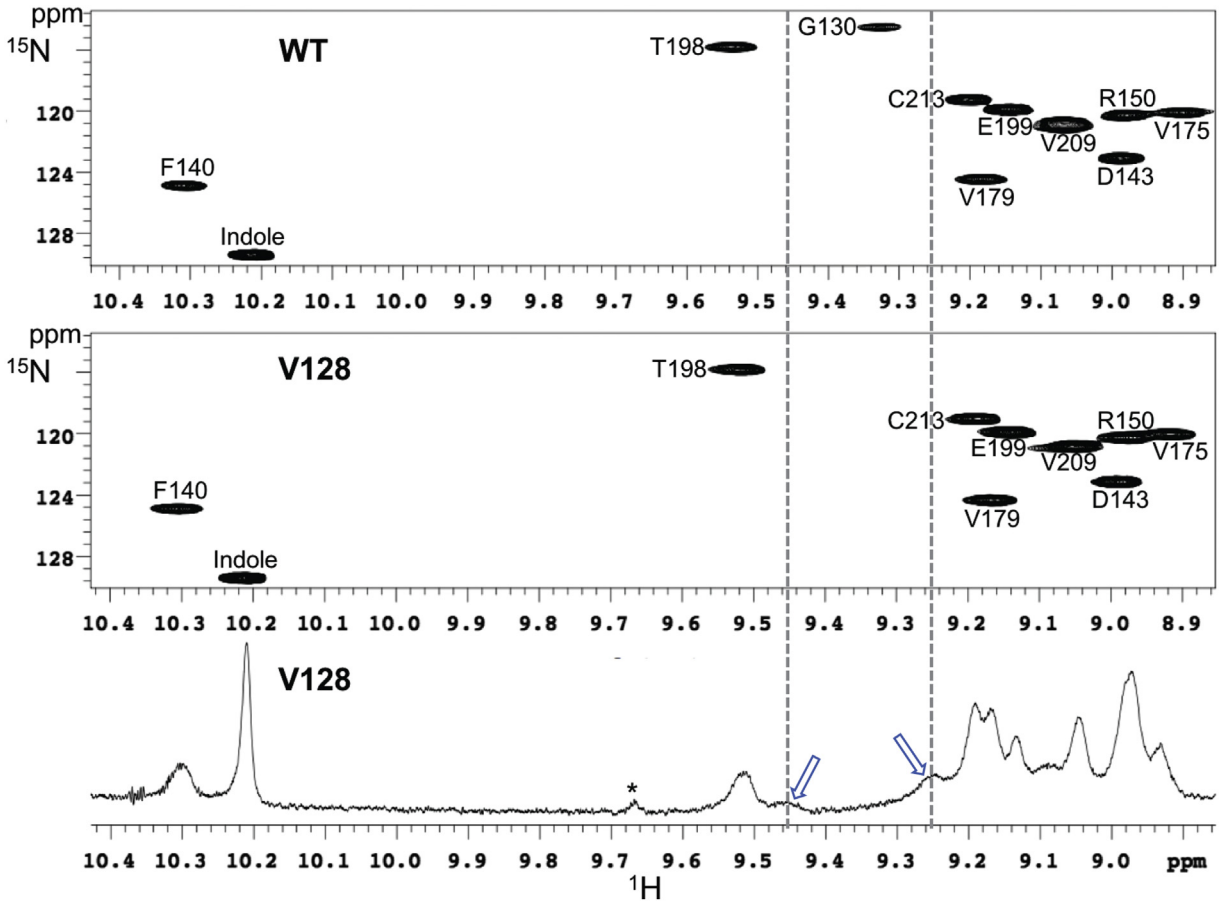

Fig. 6. 2D $^{1}H,^{15}N$-HSQC NMR spectrum for M128 (top panel), 2D $^{1}H,^{15}N$-HSQC NMR spectrum for V128 (middle panel), and 1D ^{1}H NMR spectrum of unlabeled V128 (bottom) with N-terminal his-tag removed. The arrows indicate the two resonances corresponding to the two conformations for G130; the asterisk in the 1D ^{1}H NMR spectrum indicates the resonance caused by unknown impurity.

core of a globular protein is approximated ~12 s^{-1} [19], which is close to our measured R_2 at a protein concentration of 0.1 mM (Fig. 5). Our data are consistent with previously reported R_2 values of similar length PrP constructs such as mPrP (118–231) and bovine PrP (121–231) previously reported [12,20].

When the concentration of the WT protein is ~0.2 mM, the R_2 values increased for all residues (albeit with the specific exception of residue G130, to be discussed below). Given that R_2 values are directly correlated with molecular weight and viscosity at constant temperature, these data suggest that oligomerization process takes place as the concentration of the solution increases. The increased R_2 values are consistent with the R_2 values of longer forms of PrP starting at residue 90. For instance, average R_2 values of ~15, 19, and 20 s^{-1} for residue 127–140 have been published for PrP 90–231 at concentrations of 0.5, 0.8, and 1.0 mM, respectively [21–23]. It has been inferred that presence of an N-terminal extension is correlated with increasing R_2 values; combining previously reported data with our own, it is likely that the flexible region (90–120) of PrP^{C} can enhance the PrP^{C} oligomerization process [12].

Residue G130 has a higher R_2 value than the other residues in this region, and Sullivan *et al.* [12] have suggested that it is due to chemical exchange causing broadening. An interesting observation is that the R_{ex} broadening is decreased at the higher concentrations (two-tailed test: $p = 0.074$), implying that motions at G130 near the first β-strand are altered due to the oligomerization process [24].

Polymorphism at codon 128 affects the chemical exchange at G130

G130 is located at the end of the first β-strand. In the 2D ^{1}H, ^{15}N-HSQC NMR spectra of WT allele, its resonance locates at ~115 ppm, ^{15}N dimension and ~9.3 ppm, ^{1}H dimension. However, under our experimental conditions, we noticed that in both the 2D ^{1}H, ^{15}N-HSQC NMR spectra for V128 and

HRdup, the G130 resonance is unobservable compared with WT where it is weak but observable. In the high signal-to-noise 1D ^{1}H NMR spectrum of V128 (using His-tag free non-^{13}C,^{15}N-labeled protein), we observe two resonances, one at each side of G130 in WT spectrum (Fig. 6). This is highly consistent with what was reported by Liu *et al*. [15] that there are two conformations exist for G130; the exchange between these two conformations can result in broadening of the resonance of the amide of G130 in 2D ^{1}H,^{15}N-HSQC NMR spectra, and that the separate resonances observed in the 1D ^{1}H NMR spectrum can correspond to different conformational states.

We simulated the lineshape of G130 at different exchange rates (k_{ex}) between the two conformations. Assuming the two observed peaks are from G130 in slow exchange, we found that for the lineshape of G130 changed from a broadened singlet to two separate resonances as the k_{ex} was decreased from approximately >500 to <50 s^{-1}. Therefore, under our experimental conditions, we propose that the chemical exchange at G130 is slower when a valine is at codon 128 instead of a methionine. We measured the spectrum at 500, 600, and 700 MHz to see if we could observe lineshape changes consistent with chemical exchange between these two resonances (see Supplementary Fig. S7). Small line narrowing was observed at 700 MHz, but this was not definitive possibly because the exchange was too slow.

Discussion

In the study of the HRdup protein, additional beta structure was observed involving residues VX2 and LX3 of the insert. This raises the question of how the β1–β2 sheet is formed—do residues X1–X4 or 127–130 pair with β2 (see Fig. S6), especially in light of the higher β-propensity of the former calculated by TALOS based upon the NMR chemical shifts? As described in detail in the Results section, we conclude that in the predominant structure of the HRdup protein, the structured globular C-terminal domain of HRdup has a canonical PrP^{C} structure, with a nascent β-structure in the flexible elongated HR, which we have suggested is important in the oligomerization of the protein. The reasons are summarized below: (1) all of the resonances from the insert appear without any perturbation of the resonances from the V128 protein such as residues 131–135 contiguous to β1 (Fig. 1); (2) the pattern of the R_2 values reflecting mobility would be very different especially for VX2 and LX3, which would be immobilized; (3) the chemical shifts of the β1 strand resonances in previous structures do not show a high TALOS propensity; (4) the proposed structure of a flexible β-turn segment separated from the core is consistent with the MD simulations; and (5) secondary structure predictions show β-turn propensity for the residues in the insert. Nonetheless, it is impossible to rule out exchange between the two conformations. Importantly, as this β-structure maps within protease-resistant fragments observed after thermolysin treatment of brain material from young Tg HRdup mice and proteinase K treatment of material from aged Tg HRdup mice [10], a causal relationship to pathogenesis becomes plausible.

The genotypic composition of a high-frequency Met/Val polymorphism at position 129 in the human *PRNP* gene (i.e., M/M *versus* M/V *versus* V/V) [9] has a profound impact upon the progression and manifestation of prion diseases. This effect applies irrespective of whether disease is caused by infection (from prion-contaminated food or medical products), or by germline mutation or if the disease arises in idiopathic form, as is the case for sporadic CJD. Generally, heterozygosity at this polymorphism site can lead to substantial resistance toward prion disease; for the individuals from families with inherited prion disease if with Met/Val heterozygosity at this site, the age of the disease onset is significantly later [25–27]. A spectacular example of how this polymorphism site can determine disease phenotype is the D178N germline mutation can result in genetic CJD or fatal familial insomnia depending on whether V129 or M129 polymorphisms, respectively, are present in the chromosomal allele carrying the D to N mutation in codon 178 [28].

It was previously reported by Collinge and coworkers [23] that hPrP M129 and V129 possess the same canonical PrP^{C} structure and that similar MD and stability were observed for both alleles. Our previously published results also demonstrated that mPrP M128 and V128 have the same regional stability when subjected to progressive denaturation induced with urea [10], and the results presented herein support the same canonical core structure (see above); however, the ^{15}N relaxation data for mPrP M128 (WT) and V128 displayed different exchange dynamics at G130. We presented that under our experimental condition, when a valine is present at codon 128, the conformational exchange is slower as compared with methionine. Combined with our results where we demonstrated the relationship of the altered exchange dynamics of the first β-strand and the oligomerization of PrP^{C}, we conclude that the Met/Val polymorphism at codon 128 can affect the initial oligomerization process of PrP^{C} by altering the exchange dynamics at G130, nearby the first β-strand of PrP^{C}. This can be the structural implications, change that ultimately dictates the divergent biological phenotypes of this polymorphism.

Incorporating all the aforementioned information, we hypothesize that in HRdup, with nascent β-turn structure present at the unstructured N-terminus, the

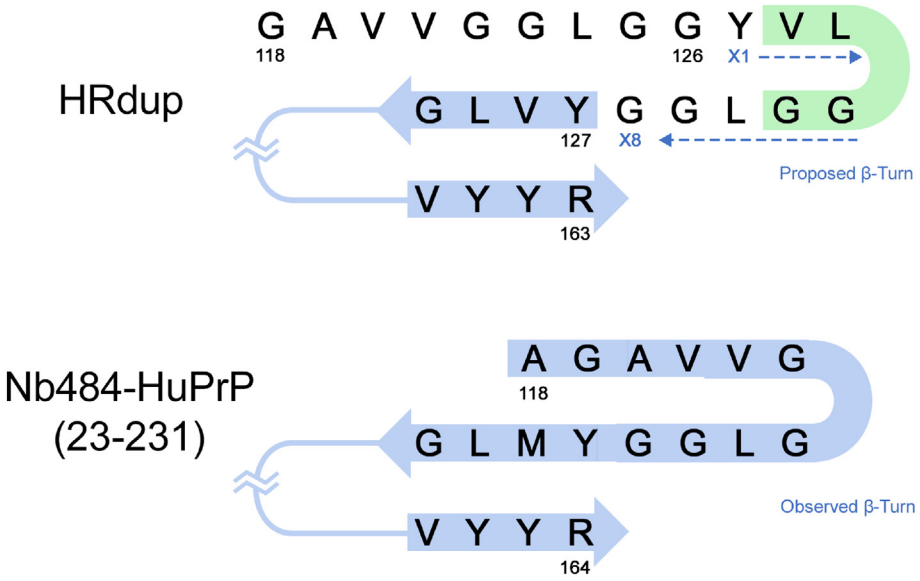

Fig. 7. At the top is the proposed misfolding-initializing structure of HRdup. The elongated HR turns, folds back, and contacts the canonical β-sheet. At the bottom is the three-strand antiparallel β-sheet structure reported by the Legname group [29].

elongated HR can spontaneously adopt a fully extended configuration and fold back to contact the existing β-sheet and altogether develop into an extended antiparallel β-structure that consists of three β-strands (Fig. 7). Such a process would be the very beginning of the misfolding and self-assembling of HRdup into a conformation high in β-structure contents. Possibly, the stacking of this proposed β-sheet structure among molecules could subsequently lead to the formation of bigger molecular assemblies and eventually, amyloids. Thus, we hypothesize that the elongated HR could be the birthplace of the misfolding of HRdup.

According to our hypothesis, the HR could be highly involved in the initialization process of PrP^{C} transforming into its infamous form PrP^{Sc}, which is consistent with the determinant effects of a few point mutations located in this otherwise highly conserved region; the drastically different downstream outcomes of these point mutations include different phenotypes of neurological diseases [30,31] and complete resistance toward prion infection [32]. Meanwhile, as the canonical anti-parallel β-sheet of PrP^{C} is incorporated into this proposed misfolding-triggering structure, this also helps explain the correlation of the dynamics of the first β-strand and the misfolding initialization process.

The proposed β-structure to be formed by HR and the existing β-sheet has already been observed by the Legname group using WT hPrP (structure shown in Fig. 7). Their elegant work demonstrated that when crystalized with nano-body at the N-terminal end, the HR of full-length hPrP adopts a fully extended conformation and forms a three-strand β-sheet with the canonical PrP^{C} anti-parallel β-sheet; most importantly, a β-turn structure was confirmed in the HR [29]. Compared with this β-structure observed in full-length human prion protein crystal, our proposed three-strand antiparallel β-sheet model for HRdup is longer thus potentially more stable, more likely to happen under biological conditions, which can explain the higher propensity for HRdup to self-transform into a β-sheet rich structure.

Bearing in mind that a protein containing the HR and the anti-parallel β-sheet (Y145stop) can form amyloids that can cause clinical prion disease with 100% attack rate [33], one can speculate that our proposed β-structure can also be an important component of a prion disease causing particle.

Materials and Methods

Protein purification

Expression constructs for moPrP (118–231), moPrP (118–231) V128, and moPrP (118–231) HRdup (referred herein to as WT, V128, and HRdup, respectively) and based on the PD444 vector were synthesized by ATUM (California, USA), with codon optimization in the sequences previously described [10]. The N-terminus of all three proteins had a histidine tag (his-tag) composed of six histidine residues plus a TEV cleavage

site (ENLYFQ/G). Extra residues before the cleavage site were added to aid identification on SDS-PAGE when removing the his-tag. The natural-abundance-isotope material was expressed and purified in standard growth media, as used previously to prepare human PrP [34]. ^{13}C and ^{15}N isotope-enriched proteins were prepared with the 1 L LB substituted with 1 L culture medium containing 1 g of $^{15}NH_4SO_4$ (Aldrich, USA), 3 g ^{13}C–glucose (Isotech Inc., USA), 1 mM $MgSO_4$ (Caledon, Canada), 0.1 mM $CaCl_2$ (Sigma-Aldrich, USA), 1 mg of biotin (Sigma-Aldrich, USA), and 100 mg of thiamine (Sigma-Aldrich, USA).

For the removal of the his-tag, unlabeled V128 lyophilized protein material was dissolved at 0.5 mg/ml with 20 mM sodium acetate (pH 5.5) and TEV (also containing a his-tag) was used at one part in 100 by mass for 3.5 h at 34 °C in the presence of 0.5 mM EDTA. After digestion was verified by SDS-PAGE, the solution was adjusted to pH 7 then loaded onto a nickel affinity column equilibrated with solution (pH 7) containing 10 mM imidazole (Sigma-Aldrich, USA), 300 mM NaCl (Fisher Scientific, USA), and 20 mM Tris–HCl (Fisher Scientific, USA); the same solution was also applied to wash out the his-tag cleaved protein. The flow-through containing the V128 protein minus his-tag was dialyzed against water and then lyophilized.

NMR samples

Two milligrams of lyophilized [^{15}N, ^{13}C]-labeled or non-labeled protein material was dissolved in 500 µl of NMR buffer comprising 95% double distilled water and 5% D_2O. The NMR buffer also contains 10 mM of sodium acetate (pH 5) and 0.25 mM of deuterated 2.2-dimethyl-2-silapentane-5-sulfonic acid (DSS-d_6), which acts as a chemical shift standard and is also used for estimating the protein concentration of the samples. The pH of the final solution was further titrated to pH 5 with microliters of 2 M hydrochloric acid, using the ^1H NMR spectrum of acetate as a pH indicator.

NMR spectroscopy

The NMR experiments were performed on 500- and 600-MHz Varian INOVA NMR and 700-MHz Agilent VNMRS spectrometers. Except for two of the 1D experiments, all the experiments were carried out at 30 °C on the 600-MHz Varian INOVA NMR spectrometer- equipped with a triple resonance probe with Z-pulsed field gradients and a computer-controlled variable temperature module for temperature regulation. All the pulse sequences used are from Biopack (VnmrJ 3.2B, Varian Inc).

The 1D spectra were acquired with 14-ppm spectral width, 1.5-s relaxation delay, and 2-s acquisition delay; 16,000 transients were required on the 500- and 600-MHz spectrometers, while 1024 transients were required on the 700-MHz spectrometer. The 2D ^1H,^{15}N-HSQC NMR spectra were acquired with the water and gNhsqc pulse sequences of Biopack (Varian) with spectral widths of 14 ppm (ω_2) and 40 ppm (ω_1), 511 and 128 complex points, respectively; 32 transients were taken with relaxation delay of 1.5 s. The 2D ^1H,^{13}C-HSQC NMR spectra were taken with spectral widths of 14 ppm (ω_2) and 80 ppm (ω_1), 511 and 320 complex points, respectively; 64 transients were taken with relaxation delay of 1.5 s. The 3D CBCA(CO)NNH and HNCACB were acquired with spectral widths of 14 ppm (ω_3), 30 ppm (ω_2), and 80 ppm (ω_1) with 511, 42, and 64 complex points, respectively; 32 scans were taken and relaxation delay was set to 1.3 s. The 3D ^{15}N-NOESYHSQC spectra were taken acquired with spectral widths of 14 ppm (ω_3), 10 ppm (ω_2), and 30 ppm (ω_1) with 511, 125, and 42 complex points, respectively; mixing time was set to 125 ms and relaxation delay was set to 1.3 s.

While the 1D ^1H spectra were processed and plotted with VnmrJ, all the 2D and 3D spectra were processed with NMRPipe and analyzed with NMRViewJ (v9.2.0-b4, One Moon Scientific) and CcpNmr (Version 2.4).

Backbone amide relaxation data

A series of 2D ^1H–^{15}N HSQC ^{15}N T_2 spectra were acquired at 60 MHz ^{15}N frequency at 30 °C using the gNhsqc pulse sequence (VnmrJ Biopack) to obtain the backbone amide relaxation data. These relaxation experiments were acquired with ^1H and ^{15}N spectral widths of 14 ppm (ω_2) and 40 ppm (ω_1), respectively, and with 2048 (t_1) * 192 (t_2) complex points. The ^{15}N-T_2 measurements were taken with relaxation delays set to 10, 30, 50, 70, 90, and 110 ms. The delay between repetitions of the pulse sequence was 4 s to ensure no sample heating. In the absence of extra relaxation measurements (such as chemical exchange), the R_2 (=$1/T_2$) values are given by:

$$R_2 = \text{Constant} \times S^2 \times \tau_M$$

where the rotational correlation time of the protein, τ_M, is the macromolecular rotational correlation time, which is proportional to the molecular weight and the order parameter S^2 for fast internal motions ranges from 0 to 1 (flexible to ordered). In the presence of fast to intermediate chemical exchange between conformations, R_2 would be enhanced [19,35]:

$$R_2 = \text{Constant} \times S^2 \times \tau_M + R_2 \text{ exchange}$$

R_2 values were obtained by fitting peak intensity from NMRViewJ *versus* time using in-house software xcrvfit with the following equations:

$$M_{xy}(t) = M_{xy}(0)e^{-t/T_2}$$
$$R_2 = 1/T_2$$

Two-tailed P value was calculated using Mathematica version 7.

Accession numbers

The NMR chemical shift assignments have been deposited in the Biological Magnetic Resonance Data Bank with accession number 27835.

CRediT authorship contribution statement

Ze-Lin Fu: Conceptualization, Data curation, Formal analysis, Investigation, Methodology, Writing - original draft, Writing - review & editing. **Peter C. Holmes:** Formal analysis, Methodology, Software, Writing - original draft. **David Westaway:** Conceptualization, Funding acquisition, Project administration, Resources, Supervision, Writing - review & editing. **Brian D. Sykes:** Conceptualization, Data curation, Formal analysis, Investigation, Methodology, Supervision, Writing - original draft, Writing - review & editing.

Acknowledgments

This work was supported by aAlberta Prion Research Institute grant RES0016340 and Canadian Institutes of Health Research grant MOP123525.

The authors thank Dr. Joanne Lemieux for kindly providing us with the TEV protease expressing vecto and Mark Miskozie for the 700 MHz NMR spectra. The authors would also like to thank Dr. Holger Wille for many insightful discussions and Dr. Lyudmyla Dorosh for providing us with the MD simulation trajectory data.

Author Contributions: Z.L.F., D.W., and B.D.S. designed the experiments. Z.L.F. prepared all the recombinant proteins. Z.L.F. and B.D.S. performed NMR experiments. Z.L.F. and P.C.H. analyzed the NMR data. Z.L.F. wrote the paper with B.D.S., D.W., and P.C.H.

Conflict of Interest: The authors declare that there are no conflicts of interest with the contents of the article.

Appendix A. Supplementary data

Supplementary data to this article can be found online at https://doi.org/10.1016/j.jmb.2019.04.027.

Received 20 December 2018;
Received in revised form 16 April 2019;
Accepted 17 April 2019
Available online 26 April 2019

Keywords:
prion protein;
GSS disease;
NMR structure;
motion dynamics;
oligomerization

Abbreviations used:
HR, hydrophobic region; GSS, Gerstmann–Sträussler–Scheinker; Tg, transgenic; WT, wild type; MD, molecular dynamics.

References

[1] S.B. Prusiner, Prions, Proc. Natl. Acad. Sci. 95 (23) (1998) 13363–13383.
[2] R.S. Sparkes, et al., Assignment of the human and mouse prion protein genes to homologous chromosomes, Proc. Natl. Acad. Sci. U. S. A. 83 (19) (Oct. 1986) 7358–7362.
[3] R. Riek, S. Hornemann, G. Wider, M. Billeter, R. Glockshuber, K. Wüthrich, NMR structure of the mouse prion protein domain PrP(121–231), Nature 382 (1996) 180–182.
[4] G.S. Jackson, et al., Location and properties of metal-binding sites on the human prion protein, Proc. Natl. Acad. Sci. U. S. A. 98 (15) (Jul. 2001) 8531–8535.
[5] G.L. Millhauser, Copper binding in the prion protein, Acc. Chem. Res. 37 (2) (2004) 79–85.
[6] B. Ghetti, et al., Gerstmann–Sträussler–Scheinker disease and the Indiana kindred, Brain Pathol. 5 (1) (1995) 61–75.
[7] S. Collins, C.A. McLean, C.L. Masters, Gerstmann–Sträussler–Scheinker syndrome, fatal familial insomnia, and kuru: a review of these less common human transmissible spongiform encephalopathies, J. Clin. Neurosci. 8 (5) (2001) 387–397.
[8] C. Hinnell, et al., Gerstmann-Sträussler-Scheinker disease due to a novel prion protein gene mutation, Neurology 76 (5) (2011) 485–487.
[9] D.M. Altshuler, et al., An integrated map of genetic variation from 1,092 human genomes, Nature 491 (7422) (2012) 56–65.
[10] R.C.C. Mercer, et al., A novel Gerstmann–Sträussler–Scheinker disease mutation defines a precursor for amyloidogenic 8 kDa PrP fragments and reveals N-Terminal structural changes shared by other GSS alleles, PLoS Pathogens 14 (2018) e1006826.
[11] T. Kitamoto, R. Iizuka, J. Tateishi, An amber mutation of prion protein in Gerstmann–Sträussler syndrome with mutant PrP plaques, Biochem. Biophys. Res. Commun. 192 (2) (Apr. 1993) 525–531.
[12] D.B.D.O. Sullivan, et al., Dynamics of a truncated prion protein, PrP(113–231), from 15N NMR relaxation: Order parameters calculated and slow conformational fluctuations localized to a distinct region, Protein Sci vol. 18 (2008) 410–423.

[13] R. Riek, S. Hornemann, G. Wider, R. Glockshuber, K. Wüthrich, NMR characterization of the full-length recombinant murine prion protein, mPrP(23–231), FEBS Lett. 413 (2) (1997) 282–288.
[14] Y. Shen, F. Delaglio, G. Cornilescu, A. Bax, TALOS+: a hybrid method for predicting protein backbone torsion angles from NMR chemical shifts, J. Biomol. NMR 44 (4) (2009) 213–223.
[15] H. Liu, et al., Solution structure of Syrian hamster prion protein rPrP(90–231), Biochemistry 38 (17) (1999) 5362–5377.
[16] D.S. Wishart, R.F. Boyko, L. Willard, F.M. Richards, B.D. Sykes, SEQSEE: a comprehensive program suite for protein sequence analysis, Comput. Appl. Biosci. 10 (2) (Apr. 1994) 121–132.
[17] H. Singh, S. Singh, G.P.S. Raghava, In silico platform for predicting and initiating β-turns in a protein at desired locations, Proteins Struct. Funct. Bioinforma. 83 (5) (2015) 910–921.
[18] G.N. Ramachan, C.M. Venkatac, Stereochemical criteria for polypeptides and proteins. IV. Standard dimensions for Cis-peptide unit and conformation of Cis-polypeptides, Biopolymers 6 (9) (1968) 1255.
[19] T.M.A. Blumenschein, D.B. Stone, R.J. Fletterick, R.A. Mendelson, B.D. Sykes, Calcium-dependent changes in the flexibility of the regulatory domain of troponin C in the troponin complex, J. Biol. Chem. 280 (23) (2005) 21924–21932.
[20] F. Lopez Garcia, R. Zahn, R. Riek, K. Wuthrich, NMR structure of the bovine prion protein, Proc. Natl. Acad. Sci. 97 (15) (2000) 8334–8339.
[21] J.H. Viles, et al., Local structural plasticity of the prion protein. Analysis of NMR relaxation, Biochemistry (2001) 2743–2753.
[22] G. Ilc, et al., NMR structure of the human prion protein with the pathological Q212P mutation reveals unique structural features, PLoS One 5 (7) (2010) 1–11.
[23] L.L.P. Hosszu, et al., The residue 129 polymorphism in human prion protein does not confer susceptibility to Creutzfeldt–Jakob disease by altering the structure or global stability of PrPc, J. Biol. Chem. 279 (27) (2004) 28515–28521.
[24] J.P. Glaves, C.L. Ladner-Keay, T.C. Bjorndahl, D.S. Wishart, B.D. Sykes, Residue-specific mobility changes in soluble oligomers of the prion protein define regions involved in aggregation, Biochim. Biophys. Acta - Proteins Proteomics 1866 (9) (2018) 982–988.
[25] M. Mullan, F. Crawford, © 199 2, Nature Publishing Grouphttp://www.nature.com/naturegenetics 1992.
[26] H.F. Baker, et al., Inherited prion disease with 144 base pair, Brain 155 (1992) 675–685.
[27] H.F. Baker, et al., Aminoacid polymorphism in human prion protein and age at death in inherited prion disease, Lancet 337 (8752) (1991) 1286.
[28] L.G. Goldfarb, et al., Fatal familial insomnia and familial Creutzfeldt–Jakob disease: disease phenotype determined by a DNA polymorphism, Science (80-.) 258 (5083) (1992) 806–808.
[29] R.N.N. Abskharon, et al., Probing the N-terminal β-sheet conversion in the crystal structure of the human prion protein bound to a nanobody, J. Am. Chem. Soc. 136 (3) (Jan. 2014) 937–944.
[30] I. Cali, et al., Impaired transmissibility of atypical prions from genetic CJD^{G114V}, Neurol. Genet. 4 (4) (2018) e253.
[31] F. Tagliavini, et al., A 7-kDa prion protein (PrP) fragment, an integral component of the PrP region required for infectivity, is the major amyloid protein in Gerstmann–Sträussler–Scheinker disease A117V, J. Biol. Chem. 276 (8) (2001) 6009–6015.
[32] E.A. Asante, et al., A naturally occurring variant of the human prion protein completely prevents prion disease, Nature 522 (7557) (Jun. 2015) 478–481.
[33] D. Aucoin, et al., Protein–solvent interfaces in human Y145Stop prion protein amyloid fibrils probed by paramagnetic solid-state NMR spectroscopy, J. Struct. Biol. (March) (2018) 1–7.
[34] R. Zahn, C. Von Schroetter, K. Wüthrich, Human prion proteins expressed in *Escherichia* cell and purified by high-affinity column refolding, FEBS Lett. 417 (3) (1997) 400–404.
[35] L.E. Kay, D.A. Torchia, A. Bax, Backbone dynamics of proteins as studied by 15N inverse detected heteronuclear NMR spectroscopy: application to staphylococcal nuclease, Biochemistry 28 (23) (1989) 8972–8979.